UK ammonia emissions estimated with satellite observations and GEOS-Chem

Eloise A. Marais[1], Alok K. Pandey[2], Martin Van Damme[3], Lieven Clarisse[3], Pierre-François Coheur[3], Mark W. Shephard[4], Karen E. Cady-Pereira[5], Tom Misselbrook[6], Lei Zhu[7], Gan Luo[8], Fangqun Yu[8]

[1]Department of Geography, University College London, London, UK.
[2] School of Physics and Astronomy, University of Leicester, Leicester, UK.
[3] Université libre de Bruxelles (ULB), Spectroscopy, Quantum Chemistry and Atmospheric Remote Sensing (SQUARES), Brussels, Belgium.
[4] Environment and Climate Change Canada, Toronto, Ontario, Canada.
[5] Atmospheric and Environmental Research (AER), Lexington, MA, USA.
[6] Department of Sustainable Agriculture Sciences, Rothamsted Research, Okehampton, UK.
[7] School of Environmental Science and Engineering, Southern University of Science and Technology, Shenzhen, China.
[8] Atmospheric Sciences Research Center, University at Albany, Albany, New York, USA.

Corresponding author: Eloise A. Marais (e.marais@ucl.ac.uk)

Key Points:

- Satellite observations of NH_3 from 2 sensors (IASI, CrIS) are used to estimate UK NH_3 emissions in Mar-Sep at fine scales (10 km, monthly)
- Satellite-derived NH_3 emissions total 272 Gg from IASI and 389 Gg from CrIS and exhibit a spring (April) and summer (July) peak
- Bottom-up emissions used for research and policy are 27-49% less than the satellite-derived estimates and miss the summer emissions peak

Abstract

Agricultural emissions of ammonia (NH_3) impact air quality, human health, and the vitality of aquatic and terrestrial ecosystems. In the UK, there are few direct policies regulating anthropogenic NH_3 emissions and development of sustainable mitigation measures necessitates reliable emissions estimates. Here we use observations of column densities of NH_3 from two space-based sensors (IASI and CrIS) with the GEOS-Chem model to derive top-down NH_3 emissions for the UK at fine spatial (~10 km) and time (monthly) scales. We focus on March-September when there is adequate spectral signal to reliably retrieve NH_3. We estimate total emissions of 272 Gg from IASI and 389 Gg from CrIS. Bottom-up emissions are 27% less than IASI and 49% less than CrIS. There are also differences in seasonality. Top-down and bottom-up emissions agree on a spring April peak due to fertilizer and manure application, but there is also a comparable summer July peak in the top-down emissions that is not in the bottom-up emissions and appears to be associated with dairy cattle farming. We estimate relative errors in the top-down emissions of 11-36% for IASI and 9-27% for CrIS, dominated by column density retrieval errors. The bottom-up versus top-down emissions discrepancies estimated in this work impact model predictions of the environmental damage caused by NH_3 emissions and warrant further investigation.

Plain Language Summary

Emissions of ammonia, mostly from agriculture, are often a dominant contributor to fine particles in countries with well-established policies that have led to large reductions in other precursors of such pollutants detrimental to our health. Here we use a model and observations of ammonia from two space-based sensors to estimate emissions in the UK where there are no direct policies regulating agricultural sources of ammonia. The satellite-derived emissions, limited to March-September when conditions are ideal for viewing ammonia from space, total 272 kilotonnes from an instrument that passes overhead in the morning and 389 kilotonnes from an instrument with a midday overpass. Though the emissions estimates differ for the two instruments, both exhibit a spring (April) peak due to fertilizer and manure use and summer (July) peak likely associated with dairy cattle farming. The summer peak is missing in bottom-up emissions and total March-September emissions from these inventories are also 27-49% less than those derived with satellites. Further research is needed to address these discrepancies, as such inventories are widely used for developing policies and assessing environmental damage caused by ammonia.

1 Introduction

Agricultural practices such as synthetic fertilizer and manure use and livestock farming release large quantities of ammonia (NH_3) to the atmosphere. Once emitted, NH_3 partitions to acidic aerosols to form ammonium that contributes to mass concentrations of fine particles ($PM_{2.5}$) hazardous to health (Cohen et al., 2017; Dockery et al., 1993; Vohra et al., 2021b). NH_3 and ammonium also deposit to the Earth's surface and drastically alter the natural nitrogen balance of terrestrial and aquatic ecosystems (Galloway, 1998; Johnson & Carpenter, 2010; Vitousek et al., 1997).

In the UK, agriculture is the dominant (>80%) source of NH_3 emissions (Ricardo, 2018b), mostly from nitrogen fertilizer use, manure management, and farming of dairy and beef cattle (DEFRA, 2019). Modelling studies suggest that the largest and most extensive decline in $PM_{2.5}$ in the UK would be achieved by targeting NH_3 sources (Vieno et al., 2016), but only large pig and poultry farms are required to adopt best practices and technologies that reduce NH_3 emissions

(DEFRA, 2019). There are additional policy options under consideration, such as limiting the use of solid urea fertilizer, a large source of NH_3 in the UK (DEFRA, 2020a). The UK is a signatory of the United Nations Economic Commission for Europe (UNECE) Gothenburg protocol, lesgislated through the UK National Emission Ceilings Regulations adopted in 2018 (UK, 2018). This commits the UK to an anthropogenic NH_3 emission ceiling of 297 Gg, informed by annual emissions estimates from the UK National Atmospheric Emissions Inventory (NAEI). The UK is also required as part of the protocol to reduce NH_3 emissions by 8% in 2020 and beyond relative to emissions in 2005 (UNECE, 2019). The estimated decline in NH_3 emissions from 1980 to 2017 is 0.2% a^{-1} due to a steep decline in vehicular emissions of NH_3 in 1998-2007 and a recent increase in agricultural emissions since 2013 mostly due to increased use of urea-based fertilizers (Ricardo, 2020). Any future policies targeting NH_3 emissions would also need to consider increases in emissions as the atmosphere warms (Sutton et al., 2013).

Estimates of the contribution of NH_3 emissions to $PM_{2.5}$ and mobilization of nitrogen in aquatic and terrestrial ecosystems, assessment of attainment of emissions ceilings commitments and targets, and decisions on effective mitigation measures demand accurate estimates of NH_3 emissions. The NAEI of annual total and mapped UK NH_3 emissions is published each year. These are obtained at high spatial resolution (1 km) with a model that uses climatological environmental factors and incorporates detailed information about farming activities that contribute to NH_3 emissions. The ability to validate the inventory is challenging, as there are no long-term measurements of NH_3 fluxes. There is a network of very reliable measurements of rural 24-hour mean surface concentrations of NH_3 that cover the full latitudinal extent of the UK from Cornwall in the south to Shetland in the north (Tang et al., 2018), but there are large monitoring gaps in-between. Individual sites are also unlikely to be representative of inventory grid cells for an emission source with large spatial variability. Satellite observations of NH_3 retrieved from infrared spectral measurements offer complete coverage of the UK and routine daily measurements in the absence of clouds and under good retrieval conditions. Satellites observe NH_3 molecules throughout the atmospheric column, but the majority are within the planetary boundary layer and most of the variability in the column is typically due to NH_3 at or near the surface (Clarisse et al., 2010; Nowak et al., 2010; Schiferl et al., 2016; Vohra et al., 2021a).

Retrieval of NH_3 from space-based instruments was first described by Beer et al. (2008) for the Tropospheric Emission Spectrometer (TES) instrument. Satellite NH_3 retrieval products have since undergone substantial retrieval development (Clarisse et al., 2009; Shephard et al., 2011; 2020; Shephard & Cady-Pereira, 2015; Van Damme et al., 2014a; 2017; 2021; Whitburn et al., 2016a), intercomparisons (Dammers et al., 2019), and validation against ground-based observations of total atmospheric column densities and surface concentrations of NH_3 (Dammers et al., 2016; 2017; Van Damme et al., 2015a; Vohra et al., 2021a). These products have also seen extensive use in characterizing NH_3 emissions. This includes detecting global and regional NH_3 emission hotspots (Cady-Pereira et al., 2017; Clarisse et al., 2019; Dammers et al., 2019; Shephard et al., 2020; Van Damme et al., 2018), constraining NH_3 emissions from biomass burning (Adams et al., 2019; Whitburn et al., 2016b), evaluating regional emission inventories (Chen et al., 2021; Fortems-Cheiney et al., 2020), identifying underestimated or missing NH_3 sources in widely used global and regional emission inventories and models (Heald et al., 2012; Hickman et al., 2018; Van Damme et al., 2014b), and determining long-term local and regional trends and variability in NH_3 (Hickman et al., 2020; Van Damme et al., 2015b; 2021; Vohra et al., 2021a).

Here we use satellite observations of NH_3 and the GEOS-Chem chemical transport model (CTM) to derive top-down NH_3 emissions for the UK and evaluate the NAEI inventory and current understanding of seasonality in emissions as represented in GEOS-Chem. This includes the use of surface observations from the UK monitoring network to evaluate the model driven with the NAEI to corroborate findings from the satellite observations.

2 Space-based observations of column densities of NH_3

Satellite observations of NH_3 retrieved in the infrared portion of the light spectrum rely on the spectral signal that depends on the atmospheric state, such as abundance and vertical distribution of NH_3 and thermal contrast between the surface of the Earth and the overlying atmosphere (Clarisse et al., 2010; Shephard et al., 2011). Two prominent products are available from contemporary space-based instruments that pass overhead in the morning (the Infrared Atmospheric Sounding Interferometer or IASI) and midday (the Cross-track Infrared Sounder or CrIS). These products use distinct retrieval approaches, offering two independent datasets to assess the potential to use satellite observations to constrain the magnitude and seasonality of UK NH_3 emissions.

2.1 Infrared Atmospheric Sounding Interferometer NH_3

The IASI instrument onboard the Metop-A satellite was launched into low-Earth polar sun synchronous orbit in October 2006. The instrument has two overpass times in the morning (09h30 local solar time or LST) and at night (21h30 LST), providing global coverage twice a day. The elliptical IASI pixels range in ground pixel resolution from 12 km × 12 km at nadir (directly below the instrument) to about 20 km × 39 km at the edges of the 2200-km-wide swath (Clarisse et al., 2011). The data product we use is the Level 2 cloud-free reanalysis product of total column NH_3 (version 3R-ERA5) (Van Damme et al., 2021). The retrieval uses machine learning, specifically a neural network trained relationship between column NH_3 and a so-called hyperspectral range index or HRI, where the HRI is a measure of the relative enhancement in the spectral signature due to NH_3 (Van Damme et al., 2014a; 2017; Whitburn et al., 2016a). The data product includes reported retrieval errors estimated by perturbing individual input parameters in the neural network framework (Whitburn et al., 2016a). Products resulting from the neural network retrieval approach have been validated against global and regional networks of ground-based NH_3 observations of surface concentrations and column densities (Dammers et al., 2016; Guo et al., 2021; Vohra et al., 2021a; Whitburn et al., 2016a). In general, IASI NH_3 reproduces the temporal variability in surface concentrations of NH_3, but exhibits a low bias (Dammers et al., 2017; Whitburn et al., 2016a).

We use daytime (09h30 LST) IASI NH_3 for 2008-2018 to obtain multiyear monthly means. This dampens influence of interannual variability and ensures consistency with NAEI NH_3 emissions that are estimated with 30-year mean meteorology (Ricardo, 2019a). We grid the data to finer spatial resolution (0.1° × 0.1°; ~ 10 km) than the native resolution of the instrument using the tessellation oversampling technique described in Zhu et al. (2017) and Sun et al. (2018). This takes advantage of the spatial variability in coverage of individual orbits and the long data record from IASI to reduce noise and smooth out spatial gradients in the gridded product (Sun et al., 2018). Briefly, tessellation involves weighting individual IASI pixels by the area of overlap with the target grid and also includes error-weighting using the reported retrieval error. In our application of the tessellation gridding technique, we approximate the area of IASI pixels as a

quadrilateral polygon, where the corners of each polygon are estimated as the distance midway between the centres of neighbouring IASI pixels.

Retrieval of NH_3 over the UK is challenging, due to persistent clouds and relatively cool conditions. Extreme retrievals, identified as absolute columns > 5×10^{17} molecules cm^{-2}, are removed. We also exclude IASI NH_3 columns retrieved on 26-27 July 2018, coincident with the summer 2018 heat wave (McCarthy et al., 2019). Record high temperatures (> 30°C) lead to UK IASI NH_3 column densities 4-times greater (~4×10^{16} molecules cm^{-2}) than the UK July multiyear mean (~1×10^{16} molecules cm^{-2}). Including these days increases the July multiyear mean by 11% and reduces its representativeness as a climatological mean for comparison to the NAEI. A similarly large influence of heat waves on IASI NH_3 columns was reported for the summer 2010 heat wave over mainland Europe (Van Damme et al., 2014b). After using oversampling to grid the data to 0.1° × 0.1°, gridded multiyear means with large relative error (>50%) are removed. This leads to loss of the majority of IASI NH_3 columns in October-February, so only March-September multiyear means are considered. Additional filtering is applied to the gridded multiyear monthly means to remove extreme values identified as columns < -1×10^{16} molecules cm^{-2} and > 1×10^{17} molecules cm^{-2}. These only account for <0.1% of the March-September data, but affect spatial consistency between IASI and CrIS.

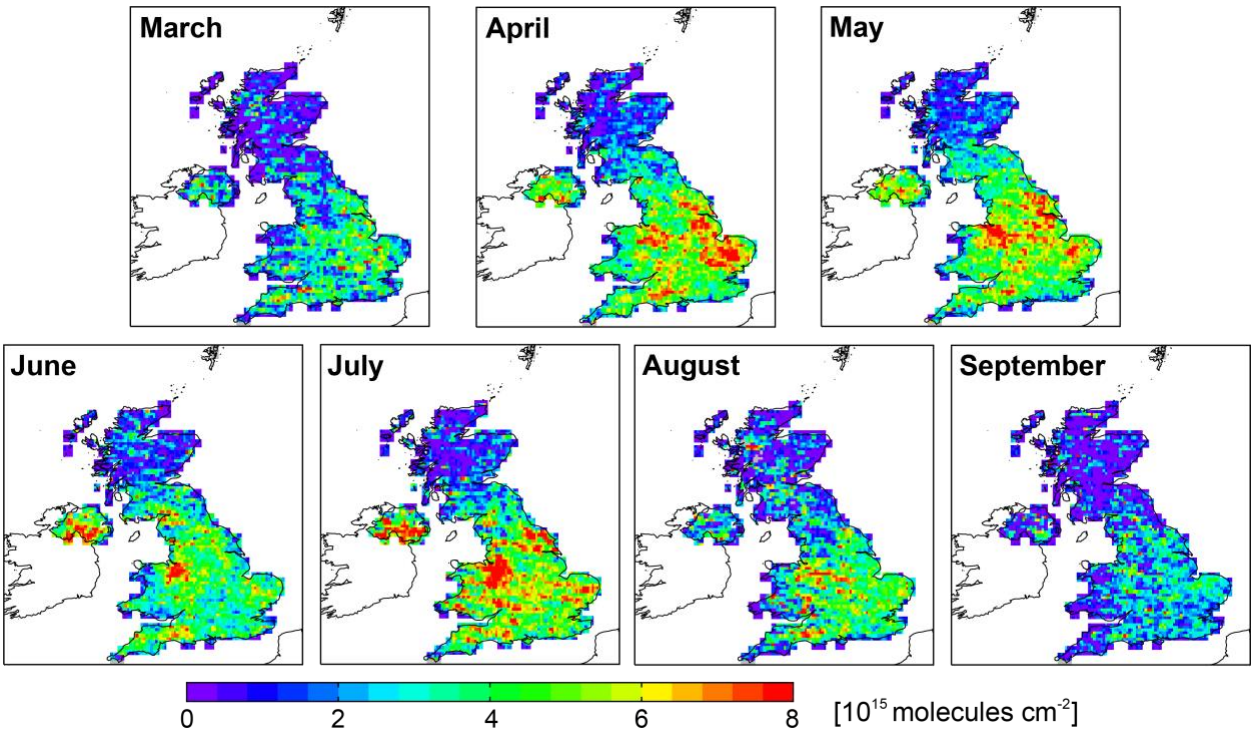

Figure 1. Monthly multiyear (2008-2018) mean IASI NH_3. Data are gridded to 0.1° × 0.1° using oversampling (see text for details). Grey grids, limited to Scotland, have < 10 observations.

Figure 1 shows the gridded March-September multiyear monthly mean IASI NH_3 columns. The number of observations in each grid ranges from 11 to 128. Values over Scotland are very low

(typically < 2×10^{15} molecules cm^{-2}) due to weak signal, lower agricultural activity than the rest of the UK, and greater distance from sources in mainland Europe. The range in IASI NH_3 over the rest of the country of 4-8 $\times 10^{15}$ molecules cm^{-2} is much less than the NH_3 hotspots in other parts of the world. Columns over global hotspots such as North China, West Africa, the Po Valley (Italy), and the Indo-Gangetic Plain (India) exceed 2×10^{16} molecules cm^{-2} (Cady-Pereira et al., 2017; Dammers et al., 2019; Van Damme et al., 2014b; 2018). These are associated with industrial and agricultural activity in India and China, and intense seasonal open burning of biomass and relatively low abundance of acidic aerosols in West Africa and northern India. Warm temperatures in these regions also increase NH_3 emissions, suppress partitioning of NH_3 to aerosols, and enhance the spectral signal.

2.2 Cross-track Infrared Sounder NH_3

The first CrIS sensor launched into low-Earth polar sun synchronous orbit in October 2011 is onboard the NOAA Suomi-NPP satellite. Like IASI, CrIS observes the Earth twice daily, though in the early afternoon (13h30 LST) and after midnight (01h30 LST) (Goldberg et al., 2013). It has the same swath width as IASI and similar ground pixel resolution (14 km circular pixels at nadir). The fast physical retrieval (CFPR) approach used to retrieve NH_3 columns is described in detail in Shephard & Cady-Pereira (2015) and Shephard et al. (2020). Briefly, it is based on conventional optimal estimation that involves minimizing the difference between observed and calculated outgoing spectral radiances with a priori vertical profiles of NH_3 (Rodgers, 2000). CFPR uses three prior NH_3 profiles representing polluted, moderately polluted, and remote conditions (Shephard et al., 2020) that are selected based on the ammonia spectral signal. This is different to standard optimal estimation that uses prior information that is independent of the observations and imposes spatial and temporal information. The CFPR retrieval generates averaging kernels that quantify the vertical sensitivity of the retrieval. These typically peak between 900 and 750 hPa (~1-2.5 km altitude) (Dammers et al., 2017; Shephard & Cady-Pereira, 2015).

We use the Level 2 CrIS NH_3 CFPR version 1.6 product for 2013-2018. The predecessor product (version 1.5) exhibited a positive bias for $NH_3 < 1 \times 10^{16}$ molecules cm^{-2}, as values were only retrieved over scenes exceeding the instrument detection limit of ~2×10^{15} molecules cm^{-2} (Dammers et al., 2017; Shephard & Cady-Pereira, 2015). This approach filtered out cloud-free scenes below the instrument detection limit and indirectly removed cloudy scenes when the NH_3 signal below clouds could not be detected. In version 1.6 clouds are explicitly identified with information from the space-based Visible Infrared Imaging Radiometer Suite (VIIRS) (White et al., 2021). We use daytime cloud-free CrIS observations with quality flag ≥ 4 (Shephard et al., 2020) and thermal contrast > 0 K, where thermal contrast is the difference between the reported temperatures at the surface and the lowest atmospheric layer. We identify and correct for a positive trend in the CrIS baseline that appears to be erroneous, as it is not apparent in the IASI data. We do this by estimating a statistically significant (p-value = 0.03) increase in monthly mean background NH_3 columns over Scotland (Figure S1) of 2.21×10^{13} molecules cm^{-2} per month (amounting to 1.6×10^{15} molecules cm^{-2} over the whole record) and subtract this from individual CrIS NH_3 column retrievals. We grid the corrected data to 0.1° × 0.1° using the same tessellation code used for IASI, but without error weighting. The individual total column errors include measurement and representative errors and cover a much narrower range (5-55% (Shephard et al., 2020)) than those for IASI (5% to >100%). As a result, higher relative weighting would be applied

to low column densities, leading to anomalously low gridded values in the CrIS multiyear means. For consistency with IASI, and because of weak spectral signal in autumn and winter, we only consider CrIS retrievals in March to September.

Figure 2 shows the gridded March-September CrIS NH_3 multiyear monthly mean columns. As with IASI, we filter for extreme values in the multiyear means (column densities < -1×10^{16} molecules cm^{-2} and > 1×10^{17} molecules cm^{-2}), removing <0.1% of the gridded data. Observations during the July 2018 heatwave only increase the July multiyear mean by 1.6%, but for consistency with IASI these days are also removed. The number of CrIS retrievals in each grid ranges from 11 to 96. The CrIS multiyear means are roughly double those for IASI (Figure 1; Figure S2), in part because CrIS passes overhead at midday when higher ambient temperatures lead to greater volatilization of NH_3. Differences in vertical sensitivity and distinct retrieval approaches likely also contribute. Difference are particularly large in September when background NH_3 is 5.3×10^{15} molecules cm^{-2} more in CrIS than IASI, obtained as the intercept from regressing CrIS against IASI. The spatial correlation between CrIS and IASI multiyear means is $R < 0.5$ in most months (March, June-September), $R = 0.53$ in May, and $R = 0.55$ in April. If extreme values in the gridded products are retained, the spatial correlation degrades to $R = 0.42$ in April and $R = 0.29$ in May.

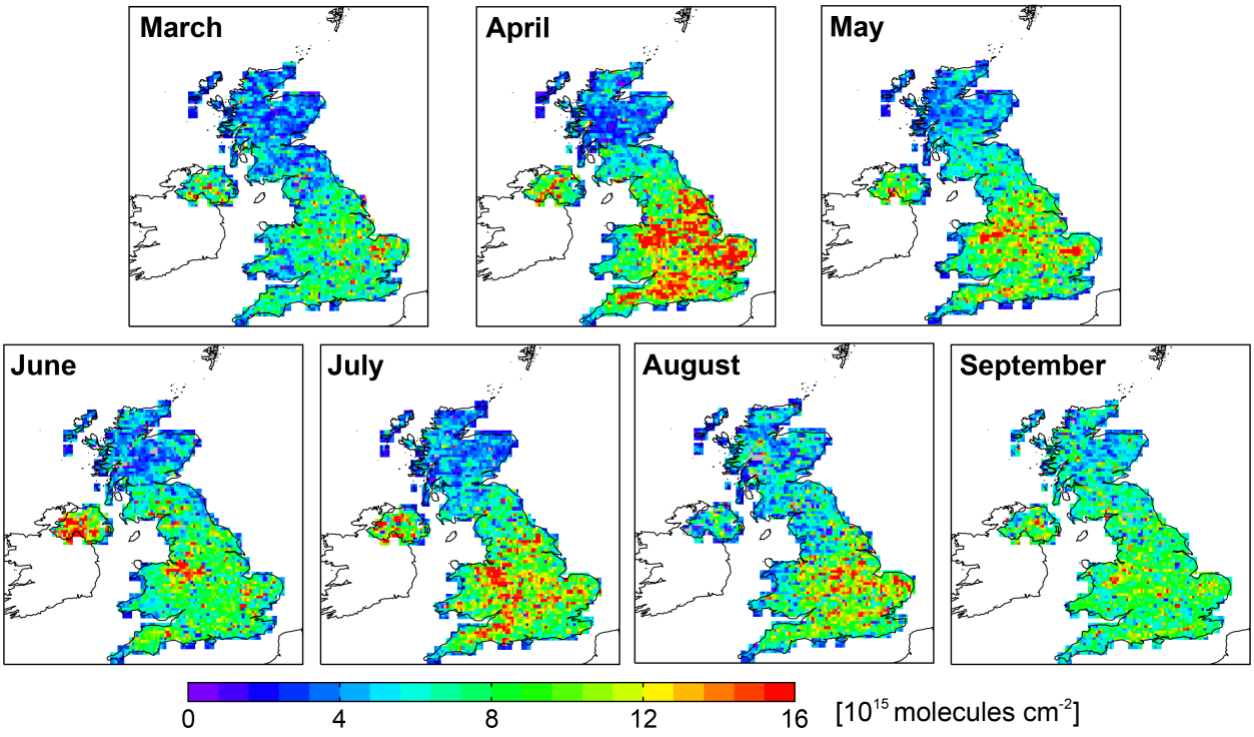

Figure 2. Monthly multiyear (2013-2018) mean CrIS NH_3. Data are gridded to 0.1° × 0.1° with oversampling (see text for details). Grey grids, limited to Scotland, have < 10 observations.

3 The GEOS-Chem chemical transport model

We use the GEOS-Chem CTM version 12.1.0 (https://doi.org/10.5281/zenodo.1553349) to derive UK NH_3 emissions from IASI and CrIS. The model is driven with NASA GEOS-FP assimilated meteorology from the Global Modeling and Assimilation Office (GMAO). Model simulations are conducted on a horizontal grid at 0.25° × 0.3125° (~25 km latitude × ~31 km longitude) nested over western Europe (32.75-61.25°N, 15°W-40°E). The model extends over 47 vertical layers from the Earth's surface to 0.01 hPa. Dynamic (3-hourly) boundary conditions are from a global GEOS-Chem simulation at 4° × 5°.

Anthropogenic emissions over the UK, including from agriculture, are updated in GEOS-Chem to include gridded emissions from the NAEI for 2016 (Ricardo, 2018a). These are annual totals on a 1 km × 1 km grid available at https://naei.beis.gov.uk/data/map-uk-das (last accessed August 2019). The agricultural NH_3 emissions incorporated in the NAEI are calculated at coarser resolution (5 km) than the NAEI with the nitrogen balance models of Webb & Misselbrook (2004) for livestock sources and Misselbrook et al. (2006) for fertilizer sources. These models are driven with 30-year mean meteorology for 1981-2010, so the NH_3 emissions represent a climatological mean (Ricardo, 2019a). Other anthropogenic NH_3 emissions in the NAEI are typically calculated as the product of emission and activity factors representative of the year of interest and mapped to the 1 km NAEI emissions grid (Ricardo, 2018b). Mainlaind Europe anthropogenic emissions for 2016 are updated with the gridded (0.1° × 0.1°) product provided by the European Monitoring and Evaluation Programme (EMEP) (http://www.ceip.at/new_emep-grid/01_grid_data; last accessed September 2019. Now at https://www.ceip.at/the-emep-grid/gridded-emissions).

Temporal variability of annual NAEI and EMEP NH_3 emissions is represented in GEOS-Chem with gridded monthly scaling factors and spatially uniform diurnal scaling factors. Monthly scaling factors are from the Generation of European Emission Data for Episodes (GENEMIS) project detailed in Friedrich (2000). These lead to peak NH_3 emissions in April. Hourly scaling factors are from Zhu et al. (2015) calculated using information about the dependence of NH_3 on aerodynamic resistance, surface temperature and Henry's law. As a result of these, 30% of NH_3 is emitted at midday (noon-2pm LST) coincident with the CrIS overpass and 20% in the morning (9am-noon LST) coincident with the IASI overpass. Natural NH_3 sources are from inventories already in GEOS-Chem. These include natural emissions from soils and the ocean from the Global Emissions InitiAtive (GEIA) inventory (Bouwman et al., 1997) and inland and coastal seabird emissions from the Riddick et al. (2012) inventory. We halve the GEIA inventory emissions, as in Paulot et al. (2014), informed by a 50% overestimate identified by Simpson et al. (1999).

NH_3 is a semi-volatile acid buffer that neutralizes acidic sulfate and nitrate aerosols, so its abundance depends on the abundance of these acidic aerosols. Sulfate forms from oxidation of SO_2 and nitrates from aerosol uptake of nitric acid formed from oxidation of NO_x. The version of the NAEI we use includes outdated mapping of the location of ships and no vertical or temporal information for aircraft emissions. To address these issues, we separate ship and aircraft emissions from other sources in the lumped "Other Transport and Mobile Machinery" category of the NAEI emissions inventory and replace ship emissions with updated estimates that use geospatial information from the automatic identification system (Ricardo, 2017). We convert the NAEI aircraft emissions to monthly estimates and distribute these vertically up to 1 km (the altitude limit of the NAEI emissions) by deriving vertical and temporal scaling factors from the global Aviation

Emissions Inventory version 2.0 (AEIv2) used in GEOS-Chem (Stettler et al., 2011). Above 1 km, the AEIv2 emissions are used. The existing temporal scaling factors in GEOS-Chem that are applied to NAEI SO_2 and NO_x emissions lead to peak emissions in winter, due to an increase in energy demand. SO_2 is emitted in the model as 95% SO_2 and 5% sulfate, using sulfate-to-SO_2 emission ratios for Europe reported by Chin et al. (2000). NAEI emissions are gridded to a uniform $0.1° \times 0.1°$ grid for input to the Harmonized Emissions Component (HEMCO) processing package version 2.1.010 (Keller et al., 2014) that maps all emissions to the model grid and applies relevant scaling factors.

The model includes detailed coupled gas- and aerosol-phase chemistry. Sulfate aerosols are formed in the model from oxidation of SO_2 in the gas phase by OH and in the aqueous phase in clouds by ozone and hydrogen peroxide (Park et al., 2004). Partitioning of NH_3 between the gas and acidic aerosol phase is determined dynamically with the thermodynamic equilibrium model ISORROPIA-II (Fountoukis & Nenes, 2007). Wet and dry deposition, terminal sinks of NH_3, are represented with a standard resistances-in-series scheme for dry deposition (Wesely, 1989) and, for wet deposition, includes scavenging in and below clouds (Amos et al., 2012).

We use network site measurements of trace gases and aerosols to evaluate model accuracy at reproducing surface concentrations of NH_3, SO_2, and sulfate. These include 2 rural sites (Auchencorth Moss in Scotland, Chilbolton Observatory in southern England) that form part of the EMEP network and the mostly rural UK Eutrophying and Acidifying Atmospheric Pollutants (UKEAP) network. The 2 EMEP sites include hourly measurements from Monitor for AeRosols and Gases in Air (MARGA) instruments (Stieger et al., 2017; ten Brink et al., 2007; Twigg et al., 2015; Walker et al., 2019). The UKEAP network includes monthly measurements from low-cost denuder filter sampling packs (Tang et al., 2018). In 2016, there were 30 sites for SO_2 and sulfate and 51 for NH_3. The MARGA data are from the EMEP Chemical Coordinating Centre EBAS database (http://ebas.nilu.no/; last accessed February 2020) (Tørseth et al., 2012) and the UKEAP data are from the UK-AIR data archive (https://uk-air.defra.gov.uk/data/data-availability; last accessed November 2020).

To ensure consistency between the model and observations, the model is sampled from the lowest to the top model layer during the satellite overpass times of 08-11 LST for use with IASI and 12-15 LST for use with CrIS, and as monthly 24-hour means in the lowest model layer for comparison to the surface observations. The model is sampled in March-September 2016 following a 2-month spin-up for chemical initialization.

4 UK bottom-up emissions of NH_3

Figure 3 shows the spatial distribution of annual UK NH_3 emissions for 2016 from the NAEI. Table 1 gives the breakdown by sector. Annual emissions for 2016 total 298 Gg, mostly (84%) from agriculture. Natural emissions of 21.6 Gg (7% of the total) are consistent with annual total natural emissions in GEOS-Chem of 21.8 Gg. According to GEOS-Chem, these include soils, vegetation and the ocean (together 18.7 Gg) and seabirds (3.10 Gg). NAEI anthropogenic NH_3 emissions total 276 Gg, 21 Gg less than the UNECE Gothenburg protocol emissions ceiling of 297 Gg (UNECE, 2019). The NAEI version we implement in GEOS-Chem and evaluate against top-down estimates was released in 2018. Two NAEI versions have been released since. Reported

differences in NH_3 emissions across these versions for consistent years is minor, just 1-3% (Ricardo, 2019b; 2020).

The spatial patterns in Figure 3 coincide with farming activities that dominate NH_3 emissions according to the modelling study by Hellsten et al. (2008). They used the same Webb & Misselbrook (2004) nitrogen balance model as the NAEI to identify regionally dominant farming activities. The agricultural sources that dominate NH_3 emissions include sheep farming along the Welsh border where emissions are low, and large sources like pig and poultry farming and fertilizer use in east England and dairy and beef cattle farming in west England and Northern Ireland. Hellsten et al. (2008) used agricultural activity data for 2000. Detailed geospatial farming activity data is confidential and publicly available data are limited to decadal maps of farming activities in England for 2000 and 2010 and annual regional and national statistics. The decadal maps suggest that locations of intensive crop and livestock farming in England are relatively unchanged (DEFRA, 2016b; a). The regional statistics document large changes in the number of livestock and the amount of nitrogen fertilizer used from 2000 to 2016 that would affect trends in emissions. In general, livestock numbers in the UK have declined by 20% for sheep, 11% for dairy and beef cattle, and 25% for pigs (DEFRA, 2020b). Poultry, specifically table chickens, have increased by 10% in the UK, with the largest increase of 42% in Northern Ireland (DEFRA, 2020b). Nitrogen-based fertilizer usage, a dominant NH_3 source in east England (Hellsten et al., 2008), declined by 19% in the UK, though the relative proportion of urea-based fertilizer has increased (Ricardo, 2020). Regional changes in nitrogen-based fertilizers range from a 3% increase in Scotland to a 37% decrease in Northern Ireland (AIC, 2020).

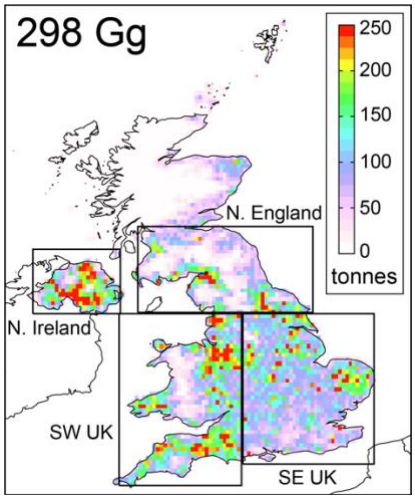

Figure 3. Annual UK NH_3 emissions for 2016. Data are in tonnes per year per 0.1° × 0.1° grid from the NAEI. Inset value is the UK annual total. Boxes demarcate regions with broadly similar NH_3 source types: Northern Ireland (N. Ireland), Northern England and a portion of southern Scotland (N. England), southwest UK (SW UK), and southeast UK (SE UK).

Table 1. UK sector emissions of NH_3 according to the NAEI [a]

Sources	**NH_3 [Gg a^{-1}]**

Agriculture	248.9
Natural [b]	21.6
Waste	14.2
Point sources	4.4
Road transport	4.4
Other [c]	4.2
Total	**297.7**

[a] Spatial distribution of UK NAEI NH_3 emissions are in Figure 3. [b] Contributors to natural emissions, according to GEOS-Chem, are soils, vegetation and the ocean (together 18.7 Gg) and seabirds (3.1 Gg). [c] Other is industrial and domestic combustion (2.9 Gg) and solvent use (1.3 Gg).

Inversion of column densities of NH_3 to estimate top-down surface emissions can be complicated by dependence of NH_3 abundance on acidic sulfate aerosols formed from oxidation of SO_2 and acidic nitrate formed from uptake of nitric acid from NO_x sources. UK SO_2 emissions are dominated by large industrial and energy sector point sources, ships, domestic and industrial combustion, and traffic (Ricardo, 2018b). UK NO_x emissions are dominated by transport, energy generation and manufacturing (Ricardo, 2018b). We find particularly large discprepancies between monthly mean March-September 2016 observed (EMEP and UKEAP) SO_2 concentrations and those from the model driven with the NAEI (Figure S3). The model normalized mean bias (NMB) is >600% for modelled $SO_2 > 2$ μg m^{-3} at sites influenced by point sources in Yorkshire and 205% for modelled $SO_2 < 2$ μg m^{-3}. Modelled sulfate is also greater than the observations (NMB of 17%) (Figure S3). This would enhance partitioning of NH_3 to acidic aerosols to form ammonium, leading to a positive bias in the relative amount of NH_x (NH_3 + ammonium) present as ammonium.

Positive model biases in both SO_2 and sulfate (Figure S3) suggest an overestimate in NAEI SO_2 emissions that have implications for UK compliance with commitments to emissions ceilings and reductions. There are many factors other than emissions that could contribute to model biases. These include, but are not limited to, misrepresentation of the height at which SO_2 is emitted from tall stacks, a reported positive bias in mainland Europe SO_2 emissions (Luo et al., 2020), and uncertainties in dry (Fowler et al., 2001; 2007) and wet (Luo et al., 2019) deposition. We conducted sensitivity simulations to assess the contribution of these uncertainties to modelled SO_2 and sulfate. Details of these simulations and the effect on SO_2 and sulfate concentrations are in the accompanying Supplementary. The factor we find to have the largest influence relative to the model bias is wet deposition. The more efficient wet deposition scheme of Luo et al. (2019) leads to an 11% decrease in sulfate concentrations.

Errors in NAEI SO_2 emissions could be due to uncertainties in emissions from domestic and industrial biomass combustion. The third of six generating units at the 3.9 GW generating capacity Drax power station in Yorkshire transitioned from burning coal to biomass in 2016 (Simet, 2017). SO_2 emissions from biomass combustion depend on fuel sulfur content and combustion efficiency. Reported emission factors range widely from 1 to 110 mg SO_2 MJ^{-1} (Boersma et al., 2008; Paulrud et al., 2006; EMEP, 2019) and so offer limited constraints. To reduce the influence of a possible bias in SO_2 emissions on GEOS-Chem simulation of abundance of sulfate and NH_3, we decrease land-based gridded ($0.1° \times 0.1°$) NAEI SO_2 emissions by a factor

of 3 for grids dominated by point sources (identified as grids with SO_2 emissions > 10 g m^{-2} a^{-1}) and by a factor of 1.3 for all other land-based grids. This reduces the original NAEI SO_2 emissions over land by 49% from 164 Gg to 84.1 Gg. With shipping, the updated annual NAEI SO_2 emissions for the domain shown in Figure 3 total 94.5 Gg. The March-September modelled sulfate NMB changes from +17% (Figure S3) to -8.8%. We use the scaled SO_2 emissions in all subsequent simulations.

5 Top-down NH_3 emissions and comparison to bottom-up estimates

We calculate gridded satellite-derived 24-hour monthly mean top-down NH_3 emissions (E_{sat}) as follows:

$$\boldsymbol{E_{sat} = \Omega_{sat} \times \left(\frac{E}{\Omega}\right)_{model}} \quad (\mathbf{1}),$$

where Ω_{sat} is satellite observations of NH_3 multiyear monthly mean columns from IASI (Figure 1) or CrIS (Figure 2), and $(E/\Omega)_{model}$ is the GEOS-Chem ratio of 24-hour monthly mean NH_3 emissions (E) to 3-hour monthly mean columns (Ω) during the satellite overpass. Model ratios ($(E/\Omega)_{model}$) are interpolated to 0.1° × 0.1°. Regression of midday vs morning values of Ω_{model} result in slopes that exceed unity (1.6-2.2), indicative of midday enhancements in NH_3 due to warmer temperatures and greater NH_3 emissions. Intercepts are small and slightly negative (-0.1 to -0.7×10^{15} molecules cm^{-2}). Regression of CrIS vs IASI Ω_{sat} yield a similar range in slopes (1.3-2.2) to the model, but large positive intercepts ($0.2\text{-}5.4 \times 10^{15}$ molecules cm^{-2}). This suggests that larger Ω_{sat} for CrIS than IASI is not just due to differences in midday and morning environmental conditions.

The mass-balance approach that we use in Eq. (1) to infer emissions can be susceptible to spatial misattribution of emissions due to displacement of NH_3 from the source. The global mean lifetime of NH_3 is ~15 h (Hauglustaine et al., 2014), ranging from ~2 h near large sources (Dammers et al., 2019) to ~36 h far from emission sources (Van Damme et al., 2018). The displacement length, the horizontal distance for the target compound to decay to ~63% of the original concentration of the emission source, provides a measure of the spatial smearing or localization error of the satellite-derived emissions (Marais et al., 2012; Palmer et al., 2003). We estimate a smearing length for satellite-derived NH_3 emissions over the UK of 10-12 km for calm conditions (wind speeds of 5-6 km h^{-1}) typical of the UK in summer (Figure A1f.3 of BEIS (2016)) and a short NH_3 lifetime typical of large sources (2 h). At slightly windier conditions (7 km h^{-1}) and over regions with lower emissions and a longer NH_3 lifetime (15 h), the displacement length increases to 105 km.

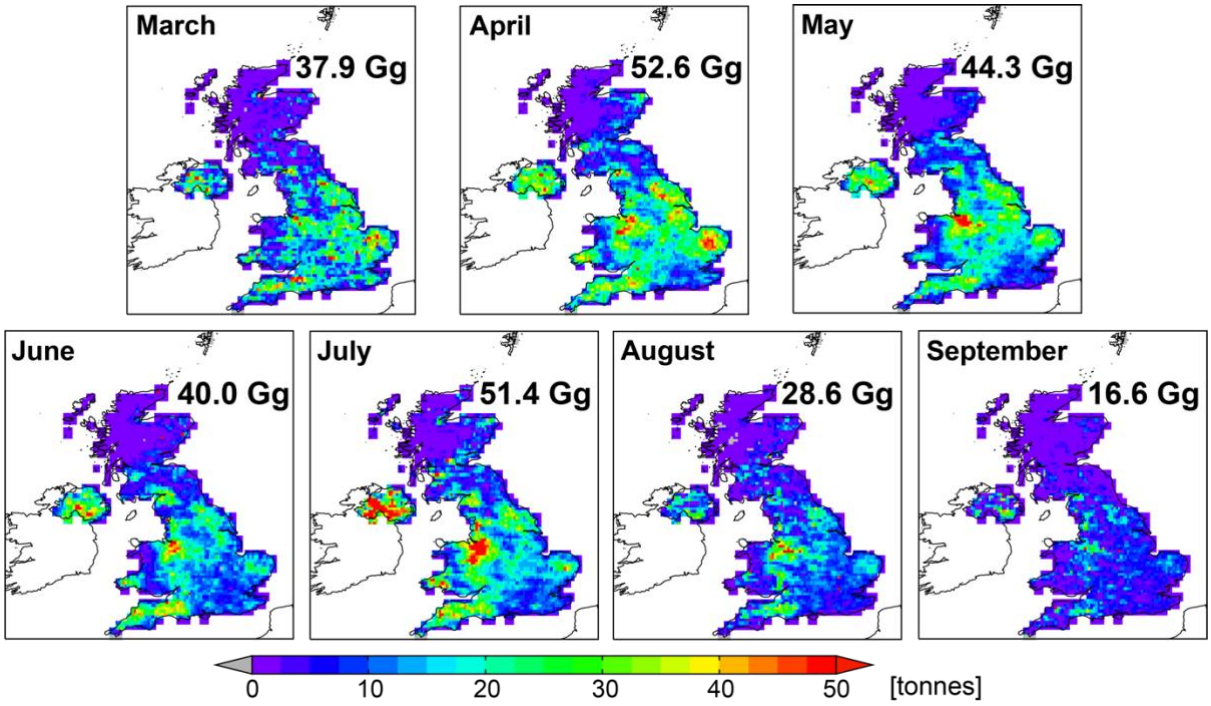

Figure 4. IASI-derived NH_3 emissions for March-September. Maps are 24-hour total emissions at 0.1° × 0.1°. Inset values are monthly emissions that sum to 271.5 Gg.

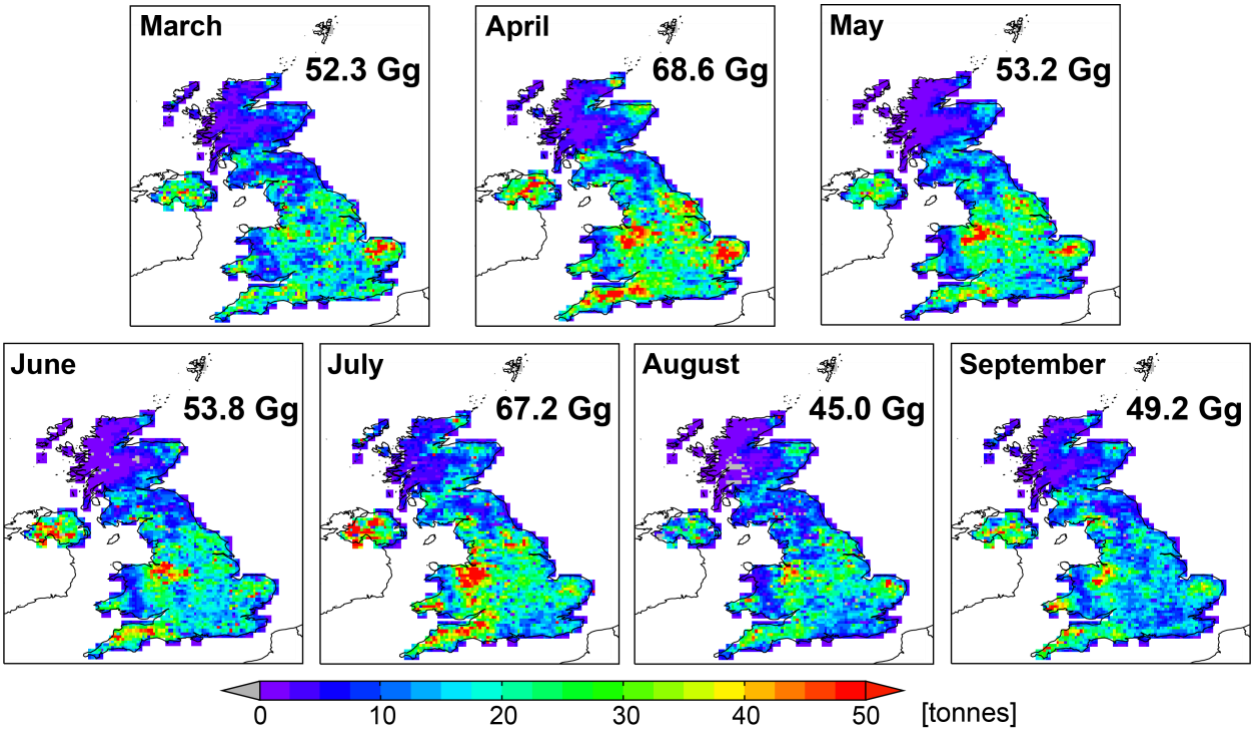

Figure 5. CrIS-derived NH_3 emissions for March-September. Maps are 24-hour total emissions at 0.1° × 0.1°. Inset values are monthly emissions that sum to 389.4 Gg.

Maps of the resultant top-down monthly NH_3 emissions are shown in Figure 4 for IASI and Figure 5 for CrIS. Qualitatively, both estimates exhibit spatial patterns similar to the NAEI (Figure 3). This includes relatively low emissions along the Welsh border, and peak emissions in Northern Ireland, the northern portion of the English side of the Welsh border, and in Norfolk in the east. Emissions for retained grid squares total 271.5 Gg for IASI, whereas these are 43% more from CrIS (389.4 Gg). CrIS monthly emissions are 20-38% more than IASI for March-July. This is similar in magnitude to the 25-50% low bias in IASI columns, though for an earlier IASI product (Dammers et al., 2017; Whitburn et al., 2016a). The percentage difference increases to 57% for August and >100% for September. The large difference in September is due to 5.4×10^{15} molecules cm^{-2} greater background NH_3 in CrIS, even after correcting for the baseline trend (Section 2.2, Figure S1). CrIS emissions excluding September are 33% more than IASI. Differences in sampling periods (2008-2018 for IASI, 2013-2018 for CrIS) only has a small effect on satellite-derived emissions, but leads to data gaps over Scotland and Northern England. IASI-derived emissions obtained for 2013-2018 are only 6% more (288.3 Gg) than those in Figure 4.

For comparison of monthly top-down and bottom-up emissions, we estimate monthly bottom-up emissions as the product of the annual NAEI emissions in Figure 3 and GEOS-Chem seasonality. The latter we obtain as ratios of GEOS-Chem monthly to annual 24-hour NH_3 emissions interpolated onto the $0.1° \times 0.1°$ grid. Figure 6 shows the resultant monthly bottom-up NH_3 emissions for April and July. The other months are in the supplementary (Figure S4). The bottom-up emissions peak in April (~14% of the annual total) coincident with fertilizer application (Hellsten et al., 2007; Paulot et al., 2014). The gridded difference between top-down and bottom-up emissions are also shown in Figure 6 for April and July and in Figure S4 for the other months. Locations where bottom-up emissions exceed those from the top-down approach (red grids) mostly occur where emissions are low. The largest difference is in July when top-down emissions are 30 Gg more (IASI) and 46 Gg more (CrIS) than the bottom-up emissions. Pronounced regional differences include lower bottom-up values in eastern England, particularly in April, where fertilizer use and pigs and poultry farming are dominant sources, as well as in western England and Northern Ireland, particularly in July, where dairy cattle farming dominates (Hellsten et al., 2008). The spatial correlation between top-down and bottom-up gridded emissions in general ranges from $R = 0.5$ to $R = 0.7$, except for IASI in September ($R = 0.34$) when dynamic range in emissions is low.

The bottom-up emissions for March-September total 198.7 Gg. This is 27% less than IASI and 49% less than CrIS. It is unlikely that the relatively low bottom-up emissions is due to the time period (1981-2020) of the 30-year meteorology used to determine agricultural NH_3 emissions for the NAEI. We find that 2-metre temperature from the NASA long-term consistent relanalysis product, Modern-Era Retrospective analysis for Research and Applications Version 2 (MERRA-2), is similar for 1981-2010 (282.750 K) and 1991-2020 (282.957 K). Bottom-up emissions in March-September are 67% of the annual total, similar to ~60% for the monthly bottom-up NH_3 emissions estimated by Hellsten et al. (2007). If we use this relative contribution (60-67%) to scale IASI and CrIS to annual totals, this suggests annual NH_3 emissions of 405-453 Gg according to IASI and 581-664 Gg according to CrIS. Subtracting the UK annual natural NH_3 emissions of ~22 Gg (Section 3) yields top-down annual anthropogenic NH_3 emissions of 383-431 Gg according to IASI and 559-642 Gg according to CrIS. Both top-down estimates exceed annual total

anthropogenic emissions from the NAEI of 276 Gg (Section 3) and the Gothenburg protocol emissions ceiling of 297 Gg.

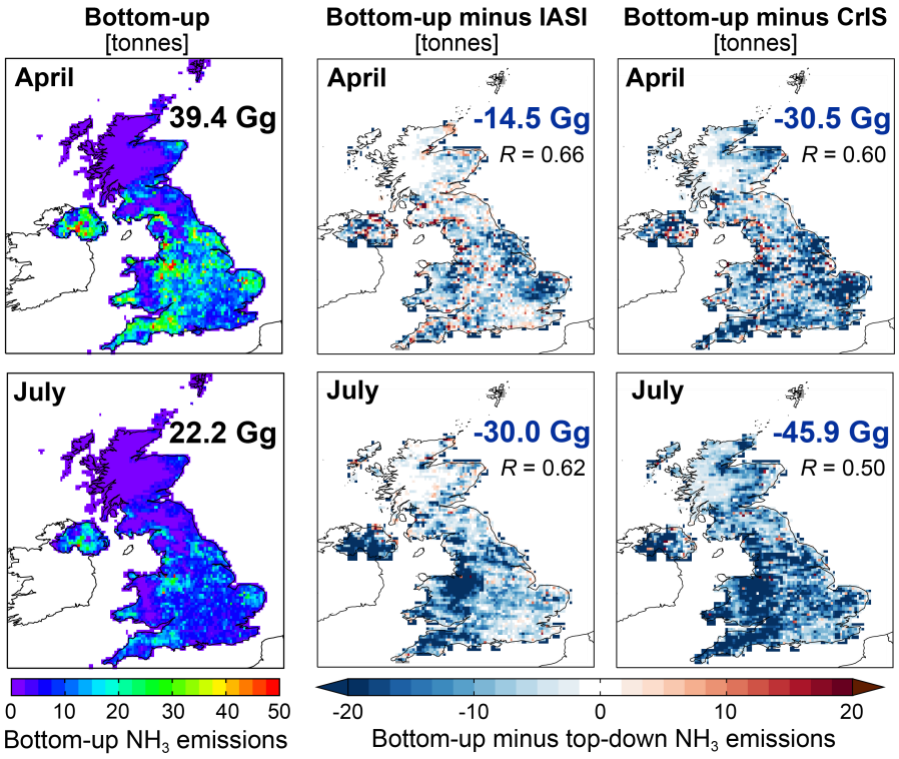

Figure 6. Comparison of bottom-up and top-down NH_3 emissions for April and July. Panels are bottom-up emissions (left), and the difference between top-down and bottom-up emissions for IASI (middle) and CrIS (right) in April (top row) and July (bottom row). Grids are blue for bottom-up < top-down and red for bottom-up > top-down. Values inset are bottom-up total (left) and differences in (middle and right) monthly emissions and the Pearson's spatial correlation (*R*) between top-down and bottom-up emissions.

Figure 7 compares regional seasonality in UK NH_3 emissions from bottom-up and top-down estimates as the percent change in emissions in each month relative to those in June. Regional seasonality in the top-down emissions is very similar in March-August in all regions except Northern Ireland. The mismatch between IASI and CrIS in September is due to the at least 2-times greater CrIS than IASI columns in that month (Section 2). The July peak in emissions in Northern Ireland is more pronounced in IASI than CrIS. This is also apparent in the seasonality in the column densities (Figure S5). Northern Ireland has experienced dramatic changes in agricultural activity that includes increases in livetock numbers of 45% for pigs and 42% for table chickens and a decline in nitrogen fertilizer of 37% from 2000 to 2016 (DEFRA, 2020b). We find though that the that top-down emissions estimates are relatively insensitive to differences in temporal coverage of the two sensors (2008-2018 for IASI, 2013-2018 for CrIS). All emission estimates exhibit a spring peak in April due to intensive fertilizer and manure application in March-April (Hellsten et al., 2007). Paulot et al. (2014) also identified this April peak in NH_3 emissions inferred from ammonium wet deposition measurements, though a recent study questions the utility

of these measurements for constraining NH_3 emissions (Tan et al., 2020). A second summer peak in the top-down emissions in July that is not present in the bottom-up emissions could be due to the timing of manure spreading, dairy farming practices, or enhanced volatilization and suppressed dry deposition due to warm summer temperatures (Hellsten et al., 2007; Sutton et al., 1994). Spatial consistency between the July top-down emissions (Figures 4 and 5) and locations dominated by emissions from dairy cattle (Hellsten et al., 2008) suggests a it is due to dairy farming, but this requires further investigation.

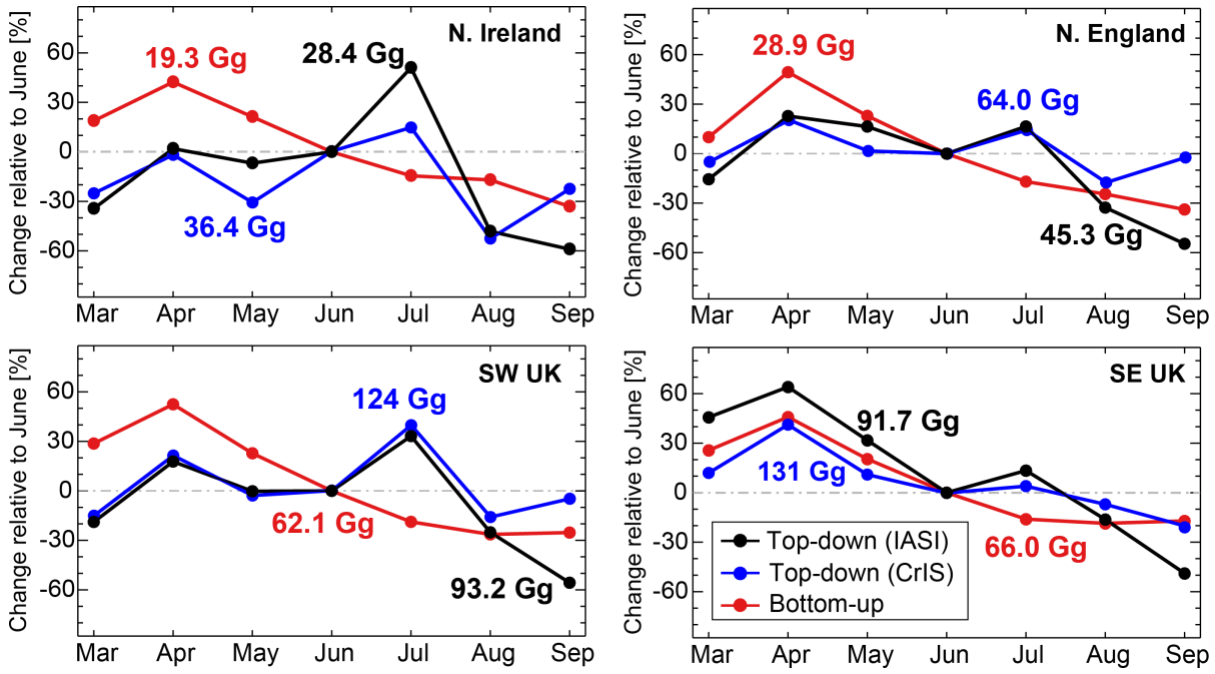

Figure 7. Regional seasonality in March-September NH_3 emissions. Points are the percentage change in emissions in each month relative to those in June for top-down emissions from IASI (black) and CrIS (blue), and from the bottom-up emissions (red). Regions sampled are in Figure 3. Inset values are March-September totals for each region from each estimate.

In Figure 8, we compare March-September 2016 mean modelled and observed surface concentrations of NH_3 to determine if the model driven with NAEI NH_3 emissions and prior assumptions of NH_3 seasonality and diurnal variability corroborates the results obtained with the satellite observations. Monthly means from model grids coincident with the surface sites are reasonably spatially consistent with the surface observations (R = 0.54) and the model is 38.3% less than the observations. This is midway between the NAEI comparison to the top-down emissions of 27% less than IASI and 49% less than CrIS. There are also low-cost passive sampler measurements of NH_3 concentrations at 39 rural sites, but these have relatively low precision, are not as extensively distributed as the observations in Figure 8, and are only reliable (within ±10%

of reference measurements) at $NH_3 \geq 2$ μg m^{-3} (Martin et al., 2019; Sutton et al., 2001). Even so, the model is similarly biased low (by 41.5%) compared to these measurements (not shown).

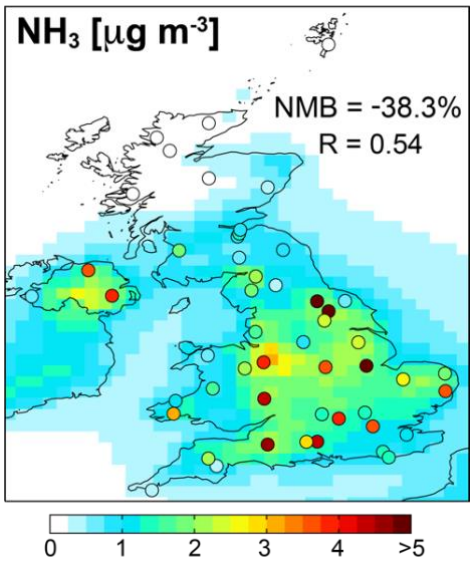

Figure 8. Comparison of observed and modelled surface concentrations of NH_3. Data are EMEP and UKEAP site measurements (points) and the model (background) for March-September 2016. Inset values are the Pearson's spatio-temporal correlation coefficient (*R*) and the model NMB for coincident monthly means.

6 Error analysis of the top-down emissions

The reported relative error for NAEI NH_3 emissions is 31% (Ricardo, 2018b). Quantifiable random errors that contribute to total March-September satellite-derived emissions include uncertainties in retrieval of NH_3, and in the modelled relationship between NH_3 emissions and column densities (Eq. (1)). For the latter we test sensitivity to modelled sulfate aerosol and nitric acid abundances and prior assumptions of the spatial and temporal variability of NH_3 emissions. IASI NH_3 retrieval errors for columns $\geq 2 \times 10^{15}$ molecules cm^{-2} range from 0.7-34%. Retrieval errors larger than 34% do occur, but are in locations with very low emissions. The CrIS NH_3 column errors across all grids range from 0.2-25%. Errors due to uncertainties in the magnitude and variability in SO_2 and NO_x emissions that affect abundance of sulfate and nitrate aerosols and hence the abundance and vertical distribution of NH_3 are small compared to column density retrieval errors. We estimate the error contribution of these as the change in top-down emissions due to a perturbation in SO_2 emissions for sulfate and NO_x emissions for nitric acid. The percent change in top-down emissions from a 50% decrease in SO_2 emissions is 4-5%. A 50% increase in NO_x emissions increases nitric acid by 14%, aerosol nitrate by 11%, and satellite-derived NH_3 emissions by 8-9%. The limited sensitivity to sulfate and nitrate in the UK is because NH_3 is in excess due to the success of emission controls targeting SO_2 and NO_x sources and absence of these for NH_3 sources. This would not occur in regions and times with large unregulated SO_2 and NO_x sources. We find that $(E/\Omega)_{\text{model}}$ used to convert satellite observations of column densities to emissions (Eq. (1)) is relatively insensitive to pertubations in NH_3 emissions, so is relatively

unaffected by errors in the spatial and temporal variability of NH_3 emissions in GEOS-Chem. A 50% increase in NH_3 emissions only causes a small (3-4%) decrease in satellite-derived NH_3 emissions. The total relative error from adding these individual errors in quadrature is 11-36% for IASI and 9-27% for CrIS and is dominated by errors in retrieval of the columns. Total emissions for March-September are 198.7 ± 61.6 Gg for the bottom-up emissions and up to 271.5 ± 97.7 Gg for IASI and 389.4 ± 105.1 Gg for CrIS.

There are also known systematic biases in the satellite observations. Some studies reported that IASI NH_3 column densities are biased low by 25-50% compared to ground-based measurements (Dammers et al., 2017; Whitburn et al., 2016a). However, these comparisons were for earlier versions of the IASI NH_3 product. The version used here is consistent with columns derived with aircraft observations (Guo et al., 2021), though Guo et al. (2021) caution that their comparison is limited in time (summer) and location (Colorado, US) and sensitive to errors in column estimates from integrating aircraft measurements. There are no observations of the vertical distribution of NH_3 over the UK. The CrIS column amounts display a gradual increase with time (Figure S1) that we correct for in this work, though further work is required to determine the cause. Biases in the satellite-derived emissions due to differences in overpass times of the two instruments is mitigated by sampling modelled columns (Ω_{model} in Eq. (1)) during the satellite overpass.

Both satellite products preferentially sample clear-sky conditions. The bias that this imparts on the top-down emissions estimates is challenging to quantify. The modelled emissions and columns used to derive top-down emissions ($(E/\Omega)_{\mathrm{model}}$ in Eq. (1)) are sampled under all-sky conditions, though there would likely be compensating effects of sampling clear-sky conditions on $(E/\Omega)_{\mathrm{model}}$. Warmer temperatures and absence of clouds increase Ω by suppressing the amount of NH_3 that partitions to the aqueous phase (Stelson & Seinfeld, 1982; Walters et al., 2018), but E_i also increases in response to warmer temperatures (Sutton et al., 2013). Preferentially sampling clear-sky conditions likely has the largest impact on Ω_{sat}. We find that the effect is greatest in July when boundary-layer clear-sky air temperatures, according to GEOS-Chem, are warmer than all-sky scenes by 5.6ºC during the morning overpass and 5.3ºC during the afternoon overpass. According to Sutton et al. (2013), 5°C warmer temperatures increase NH_3 emissions by 42%. Clear-sky temperatures are only 1.6-1.7 ºC warmer in the preceding month (June), so the greater clear-sky temperature in July may in part account for the discrepancies between observed and modelled NH_3 emissions in that month (Figure 6) and the steep increase in July columns and emissions relative to June (Figures 7 and S5). A challenge though of using GEOS-Chem to diagnose sensitivity of air temperature to cloud cover is that the model is inferior to the satellite observations at resolving clouds, due to its coarser spatial resolution (25-31 km), and only 3-12% of daily overpass model data are retained in each month after filtering for cloudy scenes (GEOS-FP cloud fractions > 0.1). NH_3 emissions in GEOS-Chem also do not include changes in farming practices in response to shifts in meteorology.

7 Conclusions

Emissions of ammonia (NH_3) in the UK are mostly (>80%) from agriculture and are challenging to estimate with bottom-up approaches and validate exclusively with current ground-based networks. Here we used satellite observations of NH_3 in March-September for multiple years from the Infrared Atmospheric Sounding Interferometer (IASI) (2008-2018) and the Cross-track

Infrared Sounder (CrIS) (2013-2018) with the GEOS-Chem chemical transport model to derive top-down monthly emissions across the UK at high spatial resolution (~10 km).

Total top-down March-September emissions are 272 Gg from IASI and 389 Gg from CrIS. Bottom-up emissions estimated with the UK National Atmospheric Emission Inventory (NAEI) annual emissions and GEOS-Chem monthly scaling factors are 27% less than IASI-derived emissions and 49% less than CrIS-derived emissions. This is supported by a 38-42% underestimate in surface NH_3 concentrations from GEOS-Chem driven with the NAEI. We infer UK top-down annual anthropogenic NH_3 emissions of 383-431 Gg from IASI and 559-642 Gg from CrIS compared to 276 Gg from the NAEI. Seasonality in the top-down emissions confirms the well-known spring April peak from fertilizer and manure use, but there is also a summer July peak coincident with intensive dairy farming that is absent in the bottom-up emissions.

The relative error in the top-down emissions, mostly due to NH_3 column retrieval errors, is 11-36% for IASI and 9-27% for CrIS and is similar to the error reported for the NAEI (31%). The top-down emissions estimates are relatively insensitive to model uncertainties in SO_2, NO_x and NH_3 emissions, as NH_3 is in excess and the relationship between modelled NH_3 columns and emissions is near-linear.

Our study demonstrates the tremendous potential to use satellite observations to derive NH_3 emissions and assess bottom-up emissions under particularly challenging observing conditions (cloudy, cool) in the UK. This is critical for assessing reliability of inventories used to inform policies and mitigation strategies. The discrepancy between bottom-up and top-down emissions identified here warrants further investigation of both approaches.

Acknowledgments, Samples, and Data

The authors are grateful for helpful discussions with Daven Henze and Hansen Cao. EAM and AKP acknowledge funding from DEFRA (contract reference ecm_55415) and EAM acknowledges additional funding from NERC/EPSRC (grant number EP/R513465/1). The research in Belgium was funded by the F.R.S.-FNRS and the Belgian State Federal Office for Scientific, Technical and Cultural Affairs (Prodex 645 arrangement IASI.FLOW). Both MVD and LC are supported by the Belgian F.R.S.-FNRS.

The top-down and bottom-up emissions estimated in this work are publicly available from the UCL Data Repository (https://doi.org/10.5522/04/14566635). The CrIS CFPR NH_3 data are created by Environment and Climate Change Canada and hosted by the Meteorological Service of Canada (MSC) Datamart. Access to the CrIS NH_3 data can be requested from MWS (mark.shephard@canada.ca). The IASI NH_3 data are publicly available from the IASI data catalogue (https://iasi.aeris-data.fr/nh3/).

References

Adams, C., McLinden, C. A., Shephard, M. W., Dickson, N., Dammers, E., Chen, J., et al. (2019), Satellite-derived emissions of carbon monoxide, ammonia, and nitrogen dioxide from the 2016 Horse River wildfire in the Fort McMurray area, *Atmospheric Chemistry and Physics*, *19*(4), 2577-2599, doi:10.5194/acp-19-2577-2019.

AIC (2020). *B2.4 Total quantities of nitrogen, phosphate and potash, UK*. Retrieved from https://www.agindustries.org.uk/static/0dd85abd-807d-4137-a00e609888633c89/Fertiliser-consumption-in-the-UK-quantity-data.pdf

Amos, H. M., Jacob, D. J., Holmes, C. D., Fisher, J. A., Wang, Q., Yantosca, R. M., et al. (2012), Gas-particle partitioning of atmospheric Hg(II) and its effect on global mercury deposition, *Atmospheric Chemistry and Physics*, *12*(1), 591-603, doi:10.5194/acp-12-591-2012.

Beer, R., Shephard, M. W., Kulawik, S. S., Clough, S. A., Eldering, A., Bowman, K. W., et al. (2008), First satellite observations of lower tropospheric ammonia and methanol, *Geophysical Research Letters*, *35*(9), L09801, doi:10.1029/2008gl033642.

BEIS (2016). *Offshore Energy Energy Strategic Environmental Assessment 3 (OESEA3) Appendix 1*. Retrieved from https://assets.publishing.service.gov.uk/government/uploads/system/uploads/attachment_data/file/504559/OESEA3_A1f_Climate___Meteorology.pdf

Boersma, A., Pels, J., Cieplik, M., van der Linden, R., Hesseling, W., & Heslinga, D. (2008). *Emissions of the use of biomass fuels in stationary applications* Retrieved from https://www.rivm.nl/bibliotheek/digitaaldepot/BOLK_I_biomass_Final.pdf

Bouwman, A. F., Lee, D. S., Asman, W. A. H., Dentener, F. J., VanderHoek, K. W., & Olivier, J. G. J. (1997), A global high-resolution emission inventory for ammonia, *Global Biogeochemical Cycles*, *11*(4), 561-587, doi:10.1029/97gb02266.

Cady-Pereira, K. E., Payne, V. H., Neu, J. L., Bowman, K. W., Miyazaki, K., Marais, E. A., et al. (2017), Seasonal and spatial changes in trace gases over megacities from Aura TES observations: two case studies, *Atmospheric Chemistry and Physics*, *17*(15), 9379-9398, doi:10.5194/acp-17-9379-2017.

Chen, Y., Shen, H., Kaiser, J., Hu, Y., Capps, S. L., Zhao, S., et al. (2021), High-resolution hybrid inversion of IASI ammonia columns to constrain US ammonia emissions using the CMAQ adjoint model, *Atmospheric Chemistry and Physics*, *21*(3), 2067-2082, doi:10.5194/acp-21-2067-2021.

Chin, M., Savoie, D. L., Huebert, B. J., Bandy, A. R., Thornton, D. C., Bates, T. S., et al. (2000), Atmospheric sulfur cycle simulated in the global model GOCART: Comparison with field observations and regional budgets, *Journal of Geophysical Research: Atmospheres*, *105*(D20), 24689-24712, doi:10.1029/2000jd900385.

Clarisse, L., Clerbaux, C., Dentener, F., Hurtmans, D., & Coheur, P.-F. (2009), Global ammonia distribution derived from infrared satellite observations, *Nature Geoscience*, *2*(7), 479-483, doi:10.1038/ngeo551.

Clarisse, L., Shephard, M. W., Dentener, F., Hurtmans, D., Cady-Pereira, K., Karagulian, F., et al. (2010), Satellite monitoring of ammonia: A case study of the San Joaquin Valley, *Journal of Geophysical Research: Atmospheres*, *115*(D13), D13302, doi:10.1029/2009jd013291.

Clarisse, L., R'Honi, Y., Coheur, P.-F., Hurtmans, D., & Clerbaux, C. (2011), Thermal infrared nadir observations of 24 atmospheric gases, *Geophysical Research Letters*, *38*(10), L10802, doi:10.1029/2011gl047271.

Clarisse, L., Van Damme, M., Clerbaux, C., & Coheur, P. F. (2019), Tracking down global NH_3 point sources with wind-adjusted superresolution, *Atmospheric Measurement Techniques*, *12*(10), 5457-5473, doi:10.5194/amt-12-5457-2019.

Cohen, A. J., Brauer, M., Burnett, R., Anderson, H. R., Frostad, J., Estep, K., et al. (2017), Estimates and 25-year trends of the global burden of disease attributable to ambient air pollution:

an analysis of data from the Global Burden of Diseases Study 2015, *The Lancet*, *389*(10082), 1907-1918, doi:10.1016/s0140-6736(17)30505-6.

Dammers, E., Palm, M., Van Damme, M., Vigouroux, C., Smale, D., Conway, S., et al. (2016), An evaluation of IASI-NH_3 with ground-based Fourier transform infrared spectroscopy measurements, *Atmospheric Chemistry and Physics*, *16*(16), 10351-10368, doi:10.5194/acp-16-10351-2016.

Dammers, E., Shephard, M. W., Palm, M., Cady-Pereira, K., Capps, S., Lutsch, E., et al. (2017), Validation of the CrIS fast physical NH_3 retrieval with ground-based FTIR, *Atmospheric Measurement Techniques*, *10*(7), 2645-2667, doi:10.5194/amt-10-2645-2017.

Dammers, E., McLinden, C. A., Griffin, D., Shephard, M. W., Van der Graaf, S., Lutsch, E., et al. (2019), NH_3 emissions from large point sources derived from CrIS and IASI satellite observations, *Atmospheric Chemistry and Physics*, *19*(19), 12261-12293, doi:10.5194/acp-19-12261-2019.

DEFRA (2016a). *Maps of livestock populations in 2000 and 2010 across England*. Retrieved from https://assets.publishing.service.gov.uk/government/uploads/system/uploads/attachment_data/file/183109/defra-stats-foodfarm-landuselivestock-june-detailedresults-livestockmaps111125.pdf

DEFRA (2016b). *Maps of crop areas in 2000 and 2010 across England*. Retrieved from https://assets.publishing.service.gov.uk/government/uploads/system/uploads/attachment_data/file/183108/defra-stats-foodfarm-landuselivestock-june-detailedresults-cropmaps111125.pdf

DEFRA (2019). *Clean Air Strategy 2019*. Retrieved from https://www.gov.uk/government/publications/clean-air-strategy-2019

DEFRA (2020a). *Consultation on reducing ammonia emissions from solid urea fertilisers*. Retrieved from https://consult.defra.gov.uk/air-quality-and-industrial-emissions/reducing-ammonia-emissions-from-urea-fertilisers/supporting_documents/Solid%20Urea%20Fertilisers%20Consultation%20Document_Nov%202020.pdf

DEFRA (2020b). *Key crop areas and livestock numbers: UK and country level data 1866-2020*. Retrieved from https://assets.publishing.service.gov.uk/government/uploads/system/uploads/attachment_data/file/946207/structure-june-ukkeyresults-22dec20.ods. Accessed on 5 January 2021.

Dockery, D. W., Pope, C. A., Xu, X., Spengler, J. D., Ware, J. H., Fay, M. E., et al. (1993), An association between air pollution and mortality in six U.S. cities, *New England Journal of Medicine*, *329*(24), 1753-1759, doi:10.1056/nejm199312093292401.

EMEP (2019). *EMEP/EEA air pollutant emission inventory guidebook 2019: 1.A.1 Energy industries*. 13/2019. Retrieved from https://www.eea.europa.eu/publications/emep-eea-guidebook-2019/part-b-sectoral-guidance-chapters/1-energy/1-a-combustion/1-a-1-energy-industries/view

Fortems-Cheiney, A., Dufour, G., Dufossé, K., Couvidat, F., Gilliot, J.-M., Siour, G., et al. (2020), Do alternative inventories converge on the spatiotemporal representation of spring ammonia emissions in France?, *Atmospheric Chemistry and Physics*, *20*(21), 13481-13495, doi:10.5194/acp-20-13481-2020.

Fountoukis, C., & Nenes, A. (2007), ISORROPIA II: a computationally efficient thermodynamic equilibrium model for K^+-Ca^{2+}-Mg^{2+}-NH_4^+-Na^+-SO_4^{2-}-NO_3^--Cl^--H_2O aerosols, *Atmospheric Chemistry and Physics*, *7*(17), 4639-4659, doi:10.5194/acp-7-4639-2007.

Fowler, D., Sutton, M. A., Flechard, C., Cape, J. N., Storeton-West, R., Coyle, M., & Smith, R. I. (2001), The control of SO_2 dry deposition on to natural surfaces by NH_3 and its effects on regional deposition, *Water, Air and Soil Pollution: Focus*, *1*(5/6), 39-48, doi:10.1023/a:1013161912231.

Fowler, D., Smith, R., Muller, J., Cape, J. N., Sutton, M., Erisman, J. W., & Fagerli, H. (2007), Long term trends in sulphur and nitrogen deposition in Europe and the cause of non-linearities, *Water, Air, & Soil Pollution: Focus*, *7*(1-3), 41-47, doi:10.1007/s11267-006-9102-x.

Fowler, D., Pilegaard, K., Sutton, M. A., Ambus, P., Raivonen, M., Duyzer, J., et al. (2009), Atmospheric composition change: Ecosystems–Atmosphere interactions, *Atmospheric Environment*, *43*(33), 5193-5267, doi:10.1016/j.atmosenv.2009.07.068.

Friedrich, R. (2000), GENEMIS: Generation of European Emission Data for Episodes, in *Transport and Chemical Transformation of Pollutants in the Troposphere*, edited by P. Borrell, Borrell, P. M. & Midgley, P., pp. 375-386, Springer-Verlag, Berlin, doi:10.1007/978-3-642-59718-3_18.

Galloway, J. N. (1998), The global nitrogen cycle: changes and consequences, *Environmental Pollution*, *102*(1), 15-24, doi:10.1016/s0269-7491(98)80010-9.

Goldberg, M. D., Kilcoyne, H., Cikanek, H., & Mehta, A. (2013), Joint Polar Satellite System: The United States next generation civilian polar-orbiting environmental satellite system, *Journal of Geophysical Research: Atmospheres*, *118*(24), 13463-13475, doi:10.1002/2013jd020389.

Guo, X., Clarisse, L., Wang, R., Van Damme, M., Whitburn, S., Coheur, P. F., et al. (2021), Validation of IASI satellite ammonia observations at the pixel scale using in-situ vertical profiles, *Journal of Geophysical Research: Atmospheres*, *126*, doi:10.1029/2020jd033475.

Hauglustaine, D. A., Balkanski, Y., & Schulz, M. (2014), A global model simulation of present and future nitrate aerosols and their direct radiative forcing of climate, *Atmospheric Chemistry and Physics*, *14*(20), 11031-11063, doi:10.5194/acp-14-11031-2014.

Heald, C. L., Collett, J. L., Lee, T., Benedict, K. B., Schwandner, F. M., Li, Y., et al. (2012), Atmospheric ammonia and particulate inorganic nitrogen over the United States, *Atmospheric Chemistry and Physics*, *12*(21), 10295-10312, doi:10.5194/acp-12-10295-2012.

Hellsten, S., Dragosits, U., Place, C. J., Misselbrook, T. H., Tang, Y. S., & Sutton, M. A. (2007), Modelling seasonal dynamics from temporal variation in agricultural practices in the UK ammonia emission inventory, *Water, Air, & Soil Pollution: Focus*, *7*(1-3), 3-13, doi:10.1007/s11267-006-9087-5.

Hellsten, S., Dragosits, U., Place, C. J., Vieno, M., Dore, A. J., Misselbrook, T. H., et al. (2008), Modelling the spatial distribution of ammonia emissions in the UK, *Environmental Pollution*, *154*(3), 370-379, doi:10.1016/j.envpol.2008.02.017.

Hickman, J. E., Dammers, E., Galy-Lacaux, C., & van der Werf, G. R. (2018), Satellite evidence of substantial rain-induced soil emissions of ammonia across the Sahel, *Atmospheric Chemistry and Physics*, *18*(22), 16713-16727, doi:10.5194/acp-18-16713-2018.

Hickman, J. E., Andela, N., Dammers, E., Clarisse, L., Coheur, P.-F., Van Damme, M., et al. (2020), Changes in biomass burning, wetland extent, or agriculture drive atmospheric NH_3 trends in several African regions, *Atmospheric Chemistry and Physics Discussions*, doi:10.5194/acp-2020-945.

Johnson, P. T. J., & Carpenter, S. R. (2010), Chapter Four. Influence of Eutrophication on Disease in Aquatic Ecosystems: Patterns, Processes, and Predictions, in *Infectious Disease Ecology*, edited by R. S. Ostfeld, Keesing, F. & Eviner, V. T., pp. 71-99, Princeton University Press, Princeton, NJ, doi:10.1515/9781400837885.71.

Keller, C. A., Long, M. S., Yantosca, R. M., Da Silva, A. M., Pawson, S., & Jacob, D. J. (2014), HEMCO v1.0: a versatile, ESMF-compliant component for calculating emissions in atmospheric models, *Geoscientific Model Development*, *7*(4), 1409-1417, doi:10.5194/gmd-7-1409-2014.

Luo, G., Yu, F. Q., & Schwab, J. (2019), Revised treatment of wet scavenging processes dramatically improves GEOS-Chem 12.0.0 simulations of surface nitric acid, nitrate, and ammonium over the United States, *Geoscientific Model Development*, *12*(8), 3439-3447, doi:10.5194/gmd-12-3439-2019.

Luo, G., Yu, F., & Moch, J. M. (2020), Further improvement of wet process treatments in GEOS-Chem v12.6.0: impact on global distributions of aerosols and aerosol precursors, *Geoscientific Model Development*, *13*(6), 2879-2903, doi:10.5194/gmd-13-2879-2020.

Makkonen, U., Virkkula, A., Mantykentta, J., Hakola, H., Keronen, P., Vakkari, V., & Aalto, P. P. (2012), Semi-continuous gas and inorganic aerosol measurements at a Finnish urban site: comparisons with filters, nitrogen in aerosol and gas phases, and aerosol acidity, *Atmospheric Chemistry and Physics*, *12*(12), 5617-5631, doi:10.5194/acp-12-5617-2012.

Marais, E. A., Jacob, D. J., Kurosu, T. P., Chance, K., Murphy, J. G., Reeves, C., et al. (2012), Isoprene emissions in Africa inferred from OMI observations of formaldehyde columns, *Atmospheric Chemistry and Physics*, *12*(14), 6219-6235, doi:10.5194/acp-12-6219-2012.

Martin, N. A., Ferracci, V., Cassidy, N., Hook, J., Battersby, R. M., di Meane, E. A., et al. (2019), Validation of ammonia diffusive and pumped samplers in a controlled atmosphere test facility using traceable Primary Standard Gas Mixtures, *Atmospheric Environment*, *199*, 453-462, doi:10.1016/j.atmosenv.2018.11.038.

McCarthy, M., Christidis, N., Dunstone, N., Fereday, D., Kay, G., Klein-Tank, A., et al. (2019), Drivers of the UK summer heatwave of 2018, *Weather*, *74*(11), 390-396, doi:10.1002/wea.3628.

Misselbrook, T. H., Sutton, M. A., & Scholefield, D. (2006), A simple process-based model for estimating ammonia emissions from agricultural land after fertilizer applications, *Soil Use and Management*, *20*(4), 365-372, doi:10.1111/j.1475-2743.2004.tb00385.x.

Nowak, J. B., Neuman, J. A., Bahreini, R., Brock, C. A., Middlebrook, A. M., Wollny, A. G., et al. (2010), Airborne observations of ammonia and ammonium nitrate formation over Houston, Texas, *Journal of Geophysical Research*, *115*(D22), D22304, doi:10.1029/2010jd014195.

Palmer, P. I., Jacob, D. J., Fiore, A. M., Martin, R. V., Chance, K., & Kurosu, T. P. (2003), Mapping isoprene emissions over North America using formaldehyde column observations from space, *Journal of Geophysical Research: Atmospheres*, *108*(D6), 4180, doi:10.1029/2002jd002153.

Park, R. J., Jacob, D. J., Field, B. D., Yantosca, R. M., & Chin, M. (2004), Natural and transboundary pollution influences on sulfate-nitrate-ammonium aerosols in the United States: Implications for policy, *Journal of Geophysical Research: Atmospheres*, *109*(D15), D15204, doi:10.1029/2003jd004473.

Paulot, F., Jacob, D. J., Pinder, R. W., Bash, J. O., Travis, K., & Henze, D. K. (2014), Ammonia emissions in the United States, European Union, and China derived by high-resolution inversion of ammonium wet deposition data: Interpretation with a new agricultural emissions inventory (MASAGE_NH3), *Journal of Geophysical Research: Atmospheres*, *119*(7), 4343-4364, doi:10.1002/2013jd021130.

Paulrud, S., Kindbom, K., & Gustafsson, T. (2006). *Emission factors and emissions from residential biomass combustion in Sweden*. Retrieved from https://www.diva-portal.org/smash/get/diva2:1184181/FULLTEXT01.pdf

Ricardo (2017). *A review of the NAEI shipping emissions methodology: Final report*. Retrieved from https://uk-air.defra.gov.uk/assets/documents/reports/cat07/1712140936_ED61406_NAEI_shipping_report_12Dec2017.pdf

Ricardo (2018a). *UK Emission Mapping Methodology: A report of the National Atmospheric Emission Inventory 2016*. Retrieved from https://uk-air.defra.gov.uk/assets/documents/reports/cat07/1812061112_MappingMethodology-for-NAEI-2016.pdf

Ricardo (2018b). *UK Informative Inventory Report (1990 to 2016)*. Retrieved from https://uk-air.defra.gov.uk/assets/documents/reports/cat07/1803161032_GB_IIR_2018_v1.2.pdf

Ricardo (2019a). *Ammonia futures: understanding implications for habitats and requirements for uptake of mitigation measures*. Retrieved from https://uk-air.defra.gov.uk/assets/documents/reports/cat09/1909040930_Ammonia_futures_Understanding_implications_for_habitats_requirements_for_uptake_of_mitigation_measures_Modelling_workshop_report.pdf

Ricardo (2019b). *UK Informative Inventory Report (1990 to 2017)*. Retrieved from https://uk-air.defra.gov.uk/assets/documents/reports/cat09/1904121008_GB_IIR_2019_v2.0.pdf

Ricardo (2020). *UK Informative Inventory Report (1990 to 2018)*. Retrieved from https://uk-air.defra.gov.uk/assets/documents/reports/cat07/2003131327_GB_IIR_2020_v1.0.pdf

Riddick, S. N., Dragosits, U., Blackall, T. D., Daunt, F., Wanless, S., & Sutton, M. A. (2012), The global distribution of ammonia emissions from seabird colonies, *Atmospheric Environment*, *55*, 319-327, doi:10.1016/j.atmosenv.2012.02.052.

Rodgers (2000), *Inverse Methods for Atmospheric Sounding - Theory and Practice*, World Scientific, River Edge, N.J., doi:10.1142/3171.

Schiferl, L. D., Heald, C. L., Van Damme, M., Clarisse, L., Clerbaux, C., Coheur, P.-F., et al. (2016), Interannual variability of ammonia concentrations over the United States: sources and implications, *Atmospheric Chemistry and Physics*, *16*(18), 12305-12328, doi:10.5194/acp-16-12305-2016.

Shephard, M. W., Cady-Pereira, K. E., Luo, M., Henze, D. K., Pinder, R. W., Walker, J. T., et al. (2011), TES ammonia retrieval strategy and global observations of the spatial and seasonal variability of ammonia, *Atmospheric Chemistry and Physics*, *11*(20), 10743-10763, doi:10.5194/acp-11-10743-2011.

Shephard, M. W., & Cady-Pereira, K. E. (2015), Cross-track Infrared Sounder (CrIS) satellite observations of tropospheric ammonia, *Atmospheric Measurement Techniques*, *8*(3), 1323-1336, doi:10.5194/amt-8-1323-2015.

Shephard, M. W., Dammers, E., Cady-Pereira, K. E., Kharol, S. K., Thompson, J., Gainariu-Matz, Y., et al. (2020), Ammonia measurements from space with the Cross-track Infrared Sounder: characteristics and applications, *Atmospheric Chemistry and Physics*, *20*(4), 2277-2302, doi:10.5194/acp-20-2277-2020.

Simet, A. (2017). *Drax reports good operational year, discusses future in biomass*. Retrieved from http://biomassmagazine.com/articles/14201/drax-reports-good-operational-year-discusses-future-in-biomass

Simpson, D., Winiwarter, W., Borjesson, G., Cinderby, S., Ferreiro, A., Guenther, A., et al. (1999), Inventorying emissions from nature in Europe, *Journal of Geophysical Research: Atmospheres*, *104*(D7), 8113-8152, doi:10.1029/98JD02747.

Stelson, A. W., & Seinfeld, J. H. (1982), Relative humidity and temperature dependence of the ammonium nitrate dissociation constant, *Atmospheric Environment*, *16*(5), 983-992, doi:10.1016/0004-6981(82)90184-6.

Stettler, M. E. J., Eastham, S., & Barrett, S. R. H. (2011), Air quality and public health impacts of UK airports. Part I: Emissions, *Atmospheric Environment*, *45*(31), 5415-5424, doi:10.1016/j.atmosenv.2011.07.012.

Stieger, B., Spindler, G., Fahlbusch, B., Müller, K., Grüner, A., Poulain, L., et al. (2017), Measurements of PM_{10} ions and trace gases with the online system MARGA at the research station Melpitz in Germany – A five-year study, *Journal of Atmospheric Chemistry*, *75*(1), 33-70, doi:10.1007/s10874-017-9361-0.

Sun, K., Zhu, L., Cady-Pereira, K., Chan Miller, C., Chance, K., Clarisse, L., et al. (2018), A physics-based approach to oversample multi-satellite, multispecies observations to a common grid, *Atmospheric Measurement Techniques*, *11*(12), 6679-6701, doi:10.5194/amt-11-6679-2018.

Sutton, M. A., Asman, W. A. H., & Schjorring, J. K. (1994), Dry deposition of reduced nitrogen, *Tellus B*, *46*(4), 255-273, doi:10.1034/j.1600-0889.1994.t01-2-00002.x.

Sutton, M. A., Miners, B., Tang, Y. S., Milford, C., Wyers, G. P., Duyzer, J. H., & Fowler, D. (2001), Comparison of low cost measurement techniques for long-term monitoring of atmospheric ammonia, *Journal of Environmental Monitoring*, *3*(5), 446-453, doi:10.1039/b102303a.

Sutton, M. A., Reis, S., Riddick, S. N., Dragosits, U., Nemitz, E., Theobald, M. R., et al. (2013), Towards a climate-dependent paradigm of ammonia emission and deposition, *Philosophical Transactions of the Royal Society B-Biological Sciences*, *368*(1621), 20130166, doi:10.1098/rstb.2013.0166.

Tan, J., Fu, J. S., & Seinfeld, J. H. (2020), Ammonia emission abatement does not fully control reduced forms of nitrogen deposition, *Proceedings of the National Academy of Sciences*, *117*(18), 9771-9775, doi:10.1073/pnas.1920068117.

Tang, Y. S., Braban, C. F., Dragosits, U., Simmons, I., Leaver, D., van Dijk, N., et al. (2018), Acid gases and aerosol measurements in the UK (1999-2015): regional distributions and trends, *Atmospheric Chemistry and Physics*, *18*(22), 16293-16324, doi:10.5194/acp-18-16293-2018.

ten Brink, H., Otjes, R., Jongejan, P., & Slanina, S. (2007), An instrument for semi-continuous monitoring of the size-distribution of nitrate, ammonium, sulphate and chloride in aerosol, *Atmospheric Environment*, *41*(13), 2768-2779, doi:10.1016/j.atmosenv.2006.11.041.

Tørseth, K., Aas, W., Breivik, K., Fjæraa, A. M., Fiebig, M., Hjellbrekke, A. G., et al. (2012), Introduction to the European Monitoring and Evaluation Programme (EMEP) and observed atmospheric composition change during 1972–2009, *Atmospheric Chemistry and Physics*, *12*(12), 5447-5481, doi:10.5194/acp-12-5447-2012.

Twigg, M. M., Di Marco, C. F., Leeson, S., van Dijk, N., Jones, M. R., Leith, I. D., et al. (2015), Water soluble aerosols and gases at a UK background site - Part 1: Controls of $PM_{2.5}$ and PM_{10} aerosol composition, *Atmospheric Chemistry and Physics*, *15*(14), 8131-8145, doi:10.5194/acp-15-8131-2015.

UK (2018). *The National Emission Ceilings Regulations 2018 (No. 129)*. Retrieved from https://www.legislation.gov.uk/uksi/2018/129/made/data.pdf

UNECE (2019). *Annex I and II of the Gothenburg Protocol*. Retrieved from https://unece.org/DAM/env/documents/2017/AIR/Gothenburg_Protocol/Annex_II_and_III_updated_clean.pdf

Van Damme, M., Clarisse, L., Heald, C. L., Hurtmans, D., Ngadi, Y., Clerbaux, C., et al. (2014a), Global distributions, time series and error characterization of atmospheric ammonia (NH_3) from IASI satellite observations, *Atmospheric Chemistry and Physics*, *14*(6), 2905-2922, doi:10.5194/acp-14-2905-2014.

Van Damme, M., Kruit, R. J. W., Schaap, M., Clarisse, L., Clerbaux, C., Coheur, P. F., et al. (2014b), Evaluating 4 years of atmospheric ammonia (NH_3) over Europe using IASI satellite observations and LOTOS-EUROS model results, *Journal of Geophysical Research: Atmospheres*, *119*(15), 9549-9566, doi:10.1002/2014jd021911.

Van Damme, M., Clarisse, L., Dammers, E., Liu, X., Nowak, J. B., Clerbaux, C., et al. (2015a), Towards validation of ammonia (NH_3) measurements from the IASI satellite, *Atmospheric Measurement Techniques*, *8*(3), 1575-1591, doi:10.5194/amt-8-1575-2015.

Van Damme, M., Erisman, J. W., Clarisse, L., Dammers, E., Whitburn, S., Clerbaux, C., et al. (2015b), Worldwide spatiotemporal atmospheric ammonia (NH_3) columns variability revealed by satellite, *Geophysical Research Letters*, *42*(20), 8660-8668, doi:10.1002/2015gl065496.

Van Damme, M., Whitburn, S., Clarisse, L., Clerbaux, C., Hurtmans, D., & Coheur, P.-F. (2017), Version 2 of the IASI NH_3 neural network retrieval algorithm: near-real-time and reanalysed datasets, *Atmospheric Measurement Techniques*, *10*(12), 4905-4914, doi:10.5194/amt-10-4905-2017.

Van Damme, M., Clarisse, L., Whitburn, S., Hadji-Lazaro, J., Hurtmans, D., Clerbaux, C., & Coheur, P. F. (2018), Industrial and agricultural ammonia point sources exposed, *Nature*, *564*(7734), 99–103, doi:10.1038/s41586-018-0747-1.

Van Damme, M., Clarisse, L., Franco, B., Sutton, M. A., Erisman, J. W., Wichink Kruit, R., et al. (2021), Global, regional and national trends of atmospheric ammonia derived from a decadal (2008-2018) satellite record, *Environmental Research Letters*, *16*(5), 055017, doi:10.1088/1748-9326/abd5e0.

Vieno, M., Heal, M. R., Williams, M. L., Carnell, E. J., Nemitz, E., Stedman, J. R., & Reis, S. (2016), The sensitivities of emissions reductions for the mitigation of UK $PM_{2.5}$, *Atmospheric Chemistry and Physics*, *16*(1), 265-276, doi:10.5194/acp-16-265-2016.

Vitousek, P. M., Aber, J. D., Howarth, R. W., Likens, G. E., Matson, P. A., Schindler, D. W., et al. (1997), Human alteration of the global nitrogen cycle: Sources and consequences, *Ecological Applications*, *7*(3), 737-750, doi:10.1890/1051-0761(1997)007[0737:Haotgn]2.0.Co;2.

Vohra, K., Marais, E. A., Suckra, S., Kramer, L., Bloss, W. J., Sahu, R., et al. (2021a), Long-term trends in air quality in major cities in the UK and India: a view from space, *Atmospheric Chemistry and Physics*, *21*(8), 6275-6296, doi:10.5194/acp-21-6275-2021.

Vohra, K., Vodonos, A., Schwartz, J., Marais, E. A., Sulprizio, M. P., & Mickley, L. J. (2021b), Global mortality from outdoor fine particle pollution generated by fossil fuel combustion: Results from GEOS-Chem, *Environmental Research*, *195*, 110754, doi:10.1016/j.envres.2021.110754.

Walker, H. L., Heal, M. R., Braban, C. F., Ritchie, S., Conolly, C., Sanocka, A., et al. (2019), Changing supersites: assessing the impact of the southern UK EMEP supersite relocation on measured atmospheric composition, *Environmental Research Communications*, *1*(0410011), doi:10.1088/2515-7620/ab1a6f.

Walters, W. W., Chai, J., & Hastings, M. G. (2018), Theoretical phase resolved ammonia–ammonium nitrogen equilibrium isotope exchange fractionations: Applications for tracking atmospheric ammonia gas-to-particle conversion, *ACS Earth and Space Chemistry*, *3*(1), 79-89, doi:10.1021/acsearthspacechem.8b00140.

Webb, J., & Misselbrook, T. H. (2004), A mass-flow model of ammonia emissions from UK livestock production, *Atmospheric Environment*, *38*(14), 2163-2176, doi:10.1016/j.atmosenv.2004.01.023.

Wesely, M. L. (1989), Parameterization of surface resistances to gaseous dry deposition in regional-scale numerical models, *Atmospheric Environment (1967)*, *23*(6), 1293-1304, doi:10.1016/0004-6981(89)90153-4.

Whitburn, S., Van Damme, M., Clarisse, L., Bauduin, S., Heald, C. L., Hadji-Lazaro, J., et al. (2016a), A flexible and robust neural network IASI-NH_3 retrieval algorithm, *Journal of Geophysical Research: Atmospheres*, *121*(11), 6581-6599, doi:10.1002/2016jd024828.

Whitburn, S., Van Damme, M., Clarisse, L., Turquety, S., Clerbaux, C., & Coheur, P. F. (2016b), Doubling of annual ammonia emissions from the peat fires in Indonesia during the 2015 El Niño, *Geophysical Research Letters*, *43*(20), 11007-11014, doi:10.1002/2016gl070620.

White, E., Shephard, M., Cady-Periera, K., Kharol, S., Dammers, E., Chow, E., et al. (2021), Accounting for non-detects in satellite retrievals: Application using CrIS ammonia observations, presented at EGU General Assembly, online, 19-30 April.

Zhu, L., Henze, D., Bash, J., Jeong, G. R., Cady-Pereira, K., Shephard, M., et al. (2015), Global evaluation of ammonia bidirectional exchange and livestock diurnal variation schemes, *Atmospheric Chemistry and Physics*, *15*(22), 12823-12843, doi:10.5194/acp-15-12823-2015.

Zhu, L., Jacob, D. J., Keutsch, F. N., Mickley, L. J., Scheffe, R., Strum, M., et al. (2017), Formaldehyde (HCHO) as a hazardous air pollutant: Mapping surface air concentrations from satellite and inferring cancer risks in the United States, *Environmental Science & Technology*, *51*(10), 5650-5657, doi:10.1021/acs.est.7b01356.